Internal Transport Barrier for Electrons in JT-60U Reversed Shear Discharges

T. Fujita, S. Ide, H. Shirai, M. Kikuchi, O. Naito, Y. Koide, S. Takeji, H. Kubo, and S. Ishida

Naka Fusion Research Establishment, Japan Atomic Energy Research Institute, Naka-machi, Naka-gun, Ibaraki-ken 311-01, Japan

(Received 29 May 1996)

A new type of internal transport barrier (ITB) has been observed in JT-60U reversed shear discharges. It accompanies clear electron temperature and density pedestals and significant reduction of effective thermal diffusivities of electrons and ions (χ_e^{eff} and χ_i^{eff}); χ_e^{eff} sharply drops by a factor of 20 within 5 cm while χ_i^{eff} is smaller than the conventional neoclassical value by a factor of 4 or more. The ratio of ion temperature to electron temperature was less than 1.5 inside the ITB. The ITB lies in the negative shear region and extended beyond 60% of the plasma minor radius. High density plasmas with high confinement have been obtained with the formation of ITB. [S0031-9007(97)02736-1]

PACS numbers: 52.55.Fa, 52.25.Fi

A reversed shear configuration, which has negative magnetic shear in the inner region and positive magnetic shear in the outer region, has been proposed as an advanced tokamak operation [1–3]. The magnetic shear is defined as $(r/q)dq/dr$, where q is the safety factor and r is the volume-averaged minor radius. The reversed shear configuration has a possibility of economical steady-state tokamak reactor with high β, good confinement, and a large bootstrap current fraction. Here, β is the ratio of plasma pressure to magnetic field pressure. In experiments, reversed shear configurations were formed by pellet injection [4], initial current ramp with neutral beam (NB) heating [5–7], off-axis lower hybrid current drive (LHCD) [8], off-axis electron cyclotron heating (ECH) [9], and so on, and confinement improvement or formation of transport barrier in the negative shear region was observed. Furthermore, internal transport barriers were observed for the ion temperature in JT-60U high β_p plasmas [10] (β_p is the ratio of plasma pressure to poloidal magnetic field pressure), which had monotonic q profiles [11].

In previous beam heating experiments [5,7,10], the reduction of the ion thermal diffusivity (χ_i) or peaking of ion temperature (T_i) profile is reported but the reduction of electron thermal diffusivity (χ_e) is not clear. In JET pellet enhanced performance mode, the reduction of χ_e is not known since the electron and ion power balances or χ_i and χ_e are not separated [12]. Clear reduction of χ_e in the negative shear region is reported in LHCD or ECH experiments [8,9]. However, it should be noted that the reduction of χ_e in these experiments is caused mainly by off-axis power deposition of lower hybrid or electron cyclotron waves rather than the spatial change of electron temperature (T_e) gradient. The inward electron heat flux (negative χ_e) was observed in DIII-D off-axis ECH experiments [13], which is considered to be due to the profile resilience. This profile resilience effect may have some contribution to the reduction of χ_e in these experiments. Though the fast wave current drive experiments with reversed shear in DIII-D [14] indicates the reduction of χ_e with on-axis heating, χ_e decreases continuously toward the axis and the effect of negative magnetic shear on χ_e profile is not clear. This Letter describes observation of a new type of internal transport barrier in the negative magnetic shear region with clear internal T_e and electron density (n_e) pedestals and with significant reduction of χ_e across the transport barrier.

The plasma configuration for JT-60U reversed shear discharges is shown in Fig. 1. Typically, the toroidal field at the plasma center (B_T) was 3.43 T, the plasma current (I_p) was 1.2 MA, and the effective surface safety factor (q_{eff} [15]) was 6.6–7.1 (q at 95% of surface poloidal flux, q_{95}, was about 5.4). The q profile was measured with motional Stark effect (MSE) diagnostics. During the period of the experiments, the MSE system [16] had five

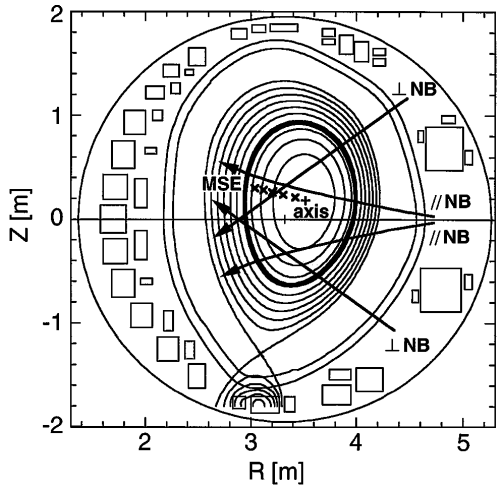

FIG. 1. Plasma configuration for reversed shear experiments. Crosses and a plus symbol denote MSE points and the magnetic axis, respectively. The thick curve denotes the flux surface at the outer edge of ITB for the profiles of Fig. 3. Trajectories of neutral beams are also shown for perpendicular ($\perp$) and tangential ($//$) injectors. The plasma major radius is 3.37 m, the plasma (horizontal) minor radius is 0.84 m, the plasma volume is 68 m^3, the ellipticity is 1.54, and the triangularity is 0.2.

viewing points and it covered a region of $R = 3.04-3.42$ m (R is the major radius). The magnetic axis (denoted by a plus symbol in Fig. 1) was located at $R = 3.5$ m and MSE viewing points (denoted by crosses) corresponded to $\rho = 0.09-0.55$ with this configuration (ρ is the normalized minor radius). The q profile was obtained by magnetohydrodynamic (MHD) equilibrium analysis using MSE data and the value of internal inductance measured with external magnetic diagnostics.

Temporal evolution of a typical discharge is shown in Fig. 2. A divertor configuration was established at $t = 3.3$ s and then injection of NB of 4 MW and the ramp of plasma current were started. The ramp rate was 0.5 MA/s and the current reached 1.2 MA at $t = 5.1$ s. During the current ramp, the NB power was increased stepwise at 4.1 s from 4 to 13 MW. This relatively high NB power during the current ramp was effective to create wide negative shear region without MHD activities. The NB powers in codirection and counterdirection (with respect to the direction of I_p) were kept nearly balanced. The deuterium gas was puffed during current ramp to increase the density up to 1.2×10^{19} m^{-3}. The NB power was increased to about 27 MW at the start of I_p flattop ($t = 5.1$ s). An H-mode transition occurred at 5.26 s and edge localized modes (ELMs) appeared at 5.32 s. Even after the ELM appearance the central density continued to rise while the edge density was kept constant as shown in Fig. 2(c), and a peaked density profile was formed. The slope of T_e profile in $\rho = 0.28-0.64$ also continued to increase as shown in Fig. 2(d). The NB power was stepped down at 5.9 s to slow down the increase of stored energy, but the central density and the pressure gradient continued to grow and the discharge reached the β limit and terminated in a disruption at 6.33 s.

Radial profiles of n_e, T_e, T_i, and q at $t = 6$ s are shown in Fig. 3. Here, n_e and T_e were measured by Thomson scattering diagnostic and T_i by charge exchange recombination spectroscopy. Steep gradients are formed at $\rho = 0.51-0.62$ in n_e and T_e profiles, which indicate the formation of internal transport barrier (ITB). The n_e and T_e gradients in the ITB are about 20 times as large as outside the ITB. In the ITB, scale lengths of n_e and T_e, $L_{ne} = -n_e/(dn_e/dr)$ and $L_{\mathrm{Te}} = -T_e/(dT_e/dr)$ are 12 and 6 cm, respectively. On the other hand, the

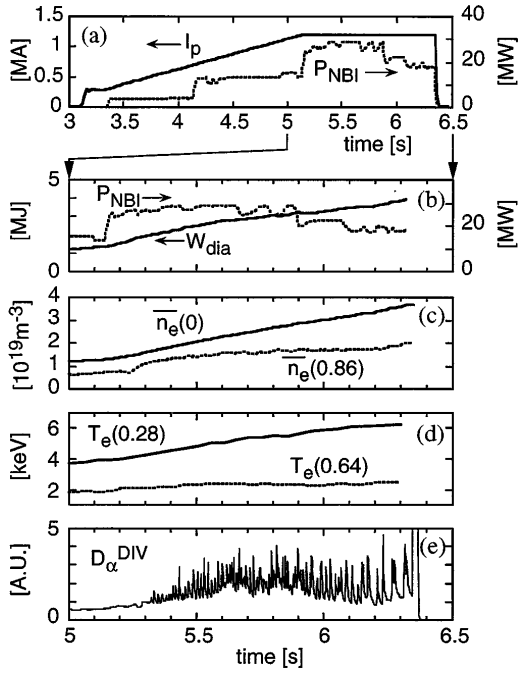

FIG. 2. Temporal evolution of a typical reversed shear discharge. (a) I_p, plasma current and P_{NBI}, injection power of neutral beam for whole discharge period. In (b) to (e), wave forms are shown for period from 5 to 6.5 s. (b) W_{dia}, stored energy and P_{NBI}. (c) $\overline{n_e}$, line-averaged density measured along $\rho = 0$ and $\rho = 0.86$. (d) $T_e(0.28)$, electron temperature at $\rho = 0.28$ and $T_e(0.64)$, electron temperature at $\rho = 0.64$. (e) D_α^{DIV}, deuterium α emission from the divertor region. Deuterium. $B_T = 3.4$ T.

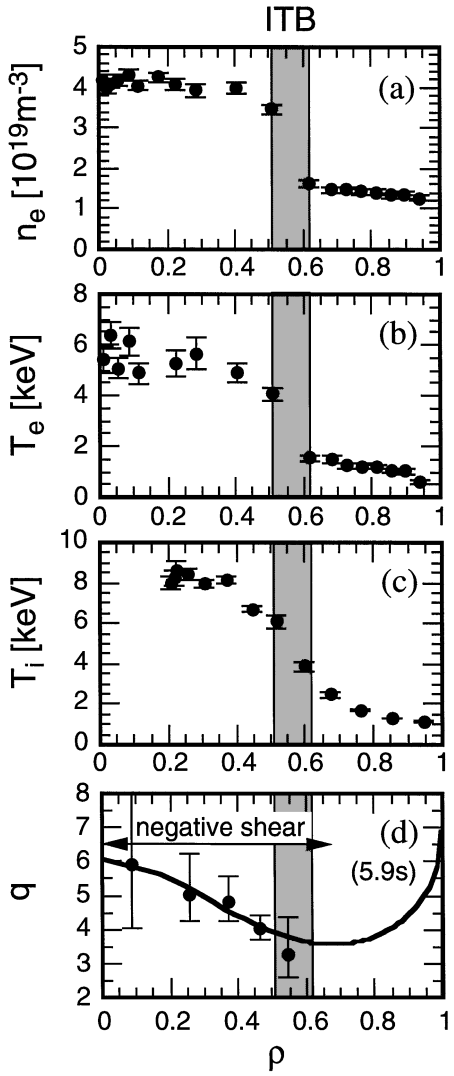

FIG. 3. Radial profiles of (a) electron density, (b) electron temperature, and (c) ion temperature at 6 s and (d) safety factor at 5.9 s of the discharge shown in Fig. 2. The volume-averaged plasma minor radius is 1.01 m.

T_i gradient changes smoothly and its scale length $L_{\mathrm{Ti}} = -T_i/(dT_i/dr)$ is larger than 19 cm. Though the spatial change of T_i gradient is not large for this shot, steeper T_i gradients were observed in other discharges. The q has its minimum value of 3.6 at $\rho = 0.67$ and the magnetic shear is negative inside it. Since there were no MSE data for $0.55 < \rho < 1$, the position of $q_{\min}$ depends on the assumption of functional form of current profile used in the analysis. The error of the position of $q_{\min}$ is estimated to be ± 0.05 according to the analysis using different functional form. Hence we can conclude that the position of outer edge of ITB is very near the position of $q_{\min}$. Inside the ITB ($\rho < 0.51$), the n_e profile is flat and the T_e and T_i gradients are small. The flux surface corresponding to the outer edge of ITB ($\rho = 0.62$) is shown by a thick curve in Fig. 1. It should be noted that the extent of negative shear region and that of improved confinement region are large; in DIII-D and TFTR reversed shear discharges the region of improved confinement was smaller or within $\rho = 0.5$ [5,6].

Transport analysis was performed for the profiles of Fig. 3. Since the carbon was dominant impurity according to spectroscopic measurements, it is assumed that the impurity ion is purely carbon. The radial profile of Z_{eff} (effective ionic charge) is assumed to be uniform since the values of Z_{eff} inside and outside the ITB were nearly equal from the measurements of Bremsstrahlung intensity profile. The value of Z_{eff} was determined to be 3.7 so as to match the calculated stored energy and neutron emission rate within 3% and 4%, respectively. This value is consistent with the value of Z_{eff} from Bremsstrahlung measurements (3.45). Orbits of fast ions and profiles of beam heating powers to bulk ions and electrons were calculated with the orbit following Monte Carlo (OFMC) code [17]. It was found that 47% of the injection power of NB was absorbed by bulk ions (30%) and electrons (17%). A substantial fraction of beam ions is lost due to ripple trapping and banana drift because of considerable toroidal field ripple (1%–1.5% at the surface) and high safety factor ($q_{\mathrm{eff}} = 6.8$) in the configuration of Fig. 1. The large ripple loss is not essential for the formation of ITB; the ITB is also obtained in the inner-shifted configuration where the ripple loss fraction is about 10%. In the transport analysis, the uncertainty in the ripple-induced loss is estimated to be $\pm 20\%$ [18]. About 70% of absorbed NB power is deposited within the ITB ($\rho < 0.62$). The deposition power profile is not peaked but rather flat within $\rho = 0.4$ since most of the beam lines do not pass the plasma center (see Fig. 1). The radial profile of radiation loss was calculated by Abel inversion of the bolometric measurements and is taken into account for the electron power balance. The time rate of change of ion and electron energy densities is calculated using n_e, T_e, and T_i profiles at 6.1 or 0.1 s after the analyzed time and is also taken into account. The results of analysis are shown in Fig. 4. Here the convective loss is included in effective thermal diffusivities of electrons and ions, χ_e^{eff} and χ_i^{eff}. The ion thermal diffusivity (without convective loss) predicted by the conventional neoclassical theory [19], χ_i^{NC} is also shown in the figure. The value of χ_e^{eff} drops sharply by a factor of 20 at $\rho = 0.62$ within 5 cm. This drop corresponds to the change of T_e gradient at the position shown in Fig. 3. On the other hand, χ_i^{eff} gradually decreases from the edge to the half radius and is smaller than the neoclassical value for $\rho < 0.6$; the upper limit of χ_i^{eff} is a quarter of the lower limit of χ_i^{NC} at $\rho = 0.45$.

The internal T_e pedestal and clear reduction of χ_e^{eff} are distinctive features and are observed for the first time in the JT-60U reversed shear discharges. Relatively low $T_i(0)/T_e(0)$ (about 1.45) was realized due to this electron transport reduction in spite of dominant ion heating by NB. Here, $T_i(0)$ and $T_e(0)$ are central ion and electron temperatures, respectively. In TFTR and DIII-D reversed shear discharges [5,7] and in JT-60U high β_ρ mode [10], mainly the ion transport was reduced and the hot ion regime [$T_i(0)/T_e(0) \geq 3$] was obtained. Though reduction of χ_e is reported in the radio-frequency wave heating experiments on Tore Supra [8], Rijnhuizen Tokamak Project [9], and DIII-D [14], no clear T_e pedestals (remarkable spatial change in L_{Te}) like the profile reported here are seen.

The ion thermal diffusivity less than the neoclassical value in TFTR reversed shear discharges is attributed to the violation of assumption of neoclassical theory (scale length of ion pressure gradient being comparable to the thermal ion banana width), thermal pinch or anomalous ion-electron thermal equilibration [5]. For

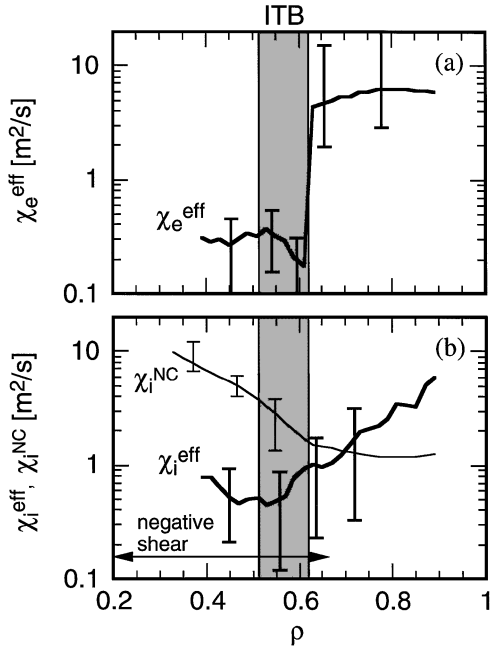

FIG. 4. Thermal diffusivities at 6 s of the discharge shown in Fig. 2: (a) effective thermal diffusivity of electron (χ_e^{eff}), (b) effective thermal diffusivity of ions (χ_i^{eff}, thick line) and ion thermal diffusivity predicted by the neoclassical theory (χ_i^{NC}, thin line).

the profiles of Fig. 3, the scale length of ion pressure gradient is 9 cm at $\rho = 0.55$. This length is close to the thermal ion banana width (5–6 cm) at that position. In addition, the large pressure gradient in the ITB is considered to cause a large radial electric field gradient, which reduces the neoclassical ion thermal diffusivity due to the orbit squeezing effect [20]. The radial electric field profile will be investigated and reported elsewhere.

In most cases, high confinement of reversed shear discharges was terminated by a collapse or sudden decrease of stored energy, which often resulted in a disruption. The collapse had no clear precursors but occurred with rapid magnetic fluctuations whose growth time was less than 50 μs. This short growth time indicates the mode is an ideal MHD instability. Low n modes such as $m/n = 3/1, 4/1, \ldots$ were dominant (m and n are poloidal and toroidal mode numbers, respectively). This collapse limited the beta value in reversed shear discharges; the discharge shown in Fig. 2 terminated in a disruption with $\beta_N = 2.02\%$ mT/MA and $\beta_p = 1.91$. Here, β_N is defined as $\beta_N = \beta \times aB_T/I_p$, a being the (horizontal) plasma minor radius. The maximum value of β_N in reversed shear plasmas with $B_T = 3.4$ T, $I_p = 1.2$ MA, and $q_{\rm eff} = 6.6$–7.1 was 2.4% mT/MA.

In Fig. 5 H factors are plotted as a function of density normalized to the Greenwald limit [21]. Here, the H factor is defined as confinement enhancement over ITER89 power law scaling [22]. In the figure, data of usual ELMy H mode in JT-60U are also shown for comparison. In usual ELMy H mode, it is necessary to increase gas puffing to raise the density, which deteriorates the energy confinement as shown in Fig. 5. In the reversed shear discharges, however, density buildup in the plasma core due to the formation of ITB results in the high density without gas puffing. Thus, we obtained high density plasmas with high confinement; the density reached 68% of the Greenwald limit, where the H factor was 2.3 and $T_i(0)/T_e(0)$ was 1.3. The maximum H factor was 2.6. Here the correction of ripple-induced loss of fast ions is not considered. Since the ripple-induced loss of fast ions is large as described above, the H factors are significantly (about 30%–40%) increased if the ripple-induced loss of fast ions is subtracted from absorption power. While low $T_i(0)/T_e(0)$ less than 1.5 was obtained in the high target density discharges like that shown in Fig. 2, higher $T_i(0)/T_e(0)$ up to 2 was also obtained in lower target density ($<0.9 \times 10^{19}$ m^{-3}) discharges.

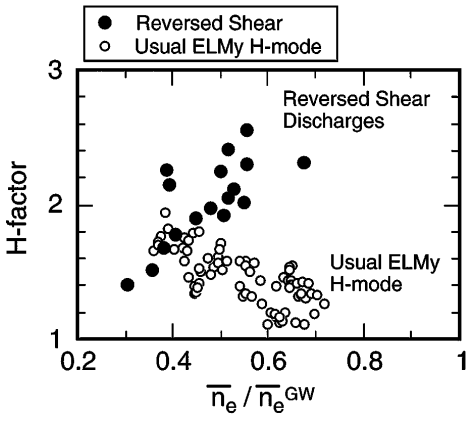

FIG. 5. Relation of H factor and the density normalized to the Greenwald limit. Closed circles denote reversed shear discharges while data for usual ELMy H mode in JT-60U are shown by small open circles for comparison.

In summary, formation of ITB with reduction of electron and ion energy transport was observed in the negative magnetic shear region in JT-60U; $\chi_e^{\rm eff}$ sharply drops by a factor of 20 within 5 cm while $\chi_i^{\rm eff}$ is less than the neoclassical value significantly. The internal T_e pedestal and clear reduction of $\chi_e^{\rm eff}$ across the ITB are observed for the first time. High density plasmas (up to 68% of Greenwald limit) with high confinement (H factor of 2.3) and with $T_i(0)/T_e(0) = 1.3$ have been obtained with the formation of ITB. This transport barrier has potential benefits for tokamak reactors which will be operated in the high density with dominant electron heating by α particles.

The authors express thanks to Dr. T. Takizuka, Dr. T. Ozeki, and Dr. Y. Kamada for useful discussions and to Dr. N. Asakura for confinement database in ELM*y H* mode.

[1] T. Ozeki *et al.*, in *Proceedings of the Fourteenth International Conference on Plasma Physics and Controlled Nuclear Fusion Research, Würzburg, 1992* (IAEA, Vienna, 1993), Vol. 2, p. 187.
[2] C. Kessel *et al.*, Phys. Rev. Lett. **72**, 1212 (1994).
[3] A. D. Turnbull *et al.*, Phys. Rev. Lett. **74**, 718 (1995).
[4] M. Hugon *et al.*, Nucl. Fusion **32**, 33 (1992).
[5] F. M. Levinton *et al.*, Phys. Rev. Lett. **75**, 4417 (1995).
[6] E. J. Strait *et al.*, Phys. Rev. Lett. **75**, 4421 (1995).
[7] B. W. Rice *et al.*, Phys. Plasmas **3**, 1983 (1996).
[8] X. Litaudon *et al.*, Plasma Phys. Controlled Fusion **38**, 1603 (1996).
[9] G. M. D. Hogeweij *et al.*, Phys. Rev. Lett. **76**, 632 (1996).
[10] Y. Koide *et al.*, Phys. Rev. Lett. **72**, 3662 (1994).
[11] S. Ishida *et al.*, in Proceedings of the Sixteenth IAEA Fusion Energy Conference, Montréal, 1996 (IAEA, Vienna, to be published).
[12] P Smeulders *et al.*, Nucl. Fusion **35**, 225 (1995).
[13] T. C. Luce *et al.*, Phys. Rev. Lett. **68**, 52 (1992).
[14] C. B. Forest *et al.*, Phys. Rev. Lett. **77**, 3141 (1996).
[15] H. Ninomiya *et al.*, Phys. Fluids B **4**, 2070 (1992).
[16] T. Fujita *et al.*, Fusion Eng. Des. (to be published).
[17] K. Tani *et al.*, J. Phys. Soc. Jpn. **50**, 1726 (1981).
[18] Y. Kusama *et al.*, in *Proceedings of the Fifteenth International Conference on Plasma Physics and Controlled Nuclear Fusion Research, Seville, 1994* (IAEA, Vienna, 1995), Vol. 1, p. 397.
[19] C. S. Chang and F. L. Hinton, Phys. Fluids **29**, 3314 (1986).
[20] K. C. Shaing and R. D. Hazeltine, Phys. Fluids B **4**, 2547 (1992).
[21] M. Greenwald *et al.*, Nucl. Fusion **28**, 2199 (1988).
[22] P. N. Yushmanov *et al.*, Nucl. Fusion **30**, 1999 (1990).